Extended Förster Theory for Determining Intraprotein Distances. 1. The κ^2-Dynamics and Fluorophore Reorientation

Pär Håkansson, Mikael Isaksson, Per-Olof Westlund, and Lennart B.-Å. Johansson*

Department of Chemistry; Biophysical Chemistry, University of Umeå, S-901 87 Umeå, Sweden

Received: June 10, 2004

A detailed analysis of the previously developed (*J. Chem. Phys.* **1996**, *105*, 10896) extended Förster theory (EFT) is presented for analyzing electronic energy migration within pairs of donors (D). Synthetic data that mimics experimental time-correlated single photon counting data were generated and re-analyzed. To cover a wide dynamic range and various orientational restrictions, the rates of reorientation, as well as the orientational configurations of the interacting D-groups were varied. In general DD distances are recovered within an error limit of 5%, while the errors in orientational configurations are usually larger. The Maier−Saupe and cone potentials were used to generate an immense variety of orientational trajectories. The results obtained exhibit no significant dependence on the choice of potential function used for generating EFT data. Present work demonstrates how to overcome the classical "κ^2-problem" and the frequently applied approximation of $\langle\kappa^2\rangle = {}^2/_3$ in the data analyses. This study also outlines the procedure for analyzing fluorescence depolarization data obtained for proteins, which are specifically labeled with D-groups. The EFT presented here brings the analyses of DDEM data to the same level of molecular detail as in ESR- and NMR-spectroscopy.

Introduction

Studies of electronic energy migration between identical fluorescent groups, the so-called donor−donor energy migration (DDEM), can give valuable information about protein structure.[1,2] Specifically, distance information between well-defined positions within a protein structure can be determined. Hitherto the analyses of such fluorescence data have been based on a model which is described in detail elsewhere.[3,4] Later a more complete theoretical analysis was derived, which in the following is referred to as the extended Förster theory (EFT).[5−7] For several reasons the EFT is more difficult to apply in the analyses of fluorescence data, which are obtained from systems like proteins. In the present paper, these difficulties are discussed and overcome. Details are given for how to use the EFT in the analyses of more complex systems.

The EFT describes energy migration within pairs of identical fluorescent groups (i.e., donors = D) that undergo reorientional motions on the time scale of interaction. This is usually the case for fluorescent D-groups covalently linked to proteins in solution. Identical fluorescent groups strictly mean that both donors exhibit the same single exponential photophysics. The rate of energy migration between interacting donors can only be obtained from fluorescence depolarization experiments. In this work, we studied the time-resolved fluorescence anisotropy, which is calculated from depolarization experiments and is in practice also the most convenient to use. Because the rates of energy migration and donor reorienting motions contribute to the fluorescence anisotropy difficulties in separating both processes are obvious. Moreover, the migration process itself depends on the reorientation of the interacting donors. The EFT provides the full description of energy migration between reorienting donors, as well as eventual changes in the distances between the interacting D-groups.[5,6] The equations of the EFT are stochastic functions, which turn out to be difficult to transform into analytical expressions. An analytical equation to apply for analyses of the depolarization data would be more straightforward.[5] Recently an approach for using the EFT principle in the analyses was developed,[6,7] but still several questions remain until the EFT can be used to analyze energy migration between donors within complex systems like proteins. At first, extensive studies have to be made on investigating the accuracy of the recovered information on distances and configurations of interacting donors undergoing different rates of restricted reorientations. This is intimately related to the well-known "κ^2-problem" frequently discussed in the literature.[8] This problem constitutes two questions: namely, to determine the mutual orientation of the interacting donors,[9] as well as its dynamics,[5] which depends on the local reorientation of the donors.

In the modeling of the stochastic functions of donor reorientation, one needs to use simulation methods, such as Brownian dynamics (BD) simulations. Because different models can be used, it is important to examine whether the choice of orienting potential is crucial for the resulting analyses. This question was studied by comparing the cone and the Maier−Saupe potential models.

Computational Methods

Brownian diffusion (BD) simulations were performed to mimic the molecular motions of donors attached to a protein. In the simulations, a unit vector representing the molecular electronic transition dipole moment ($\hat{\mu}$) undergoes restricted diffusion on a sphere, while existing within a cone potential.[6,7] To test an eventual model dependence of the extracted parameters, cone-potentials were compared to various Maier−Saupe potentials.[10−12] Common features of the simulations are listed below as well as relevant properties of the different reorientational models. To describe the motions of the molecular

* Corresponding author. E-mail: Lennart.Johansson@chem.umu.se. Telephone:+46-90-786 5149. Fax: +46-90-786 7779.

10.1021/jp040423d CCC: $27.50
Published on Web 10/08/2004

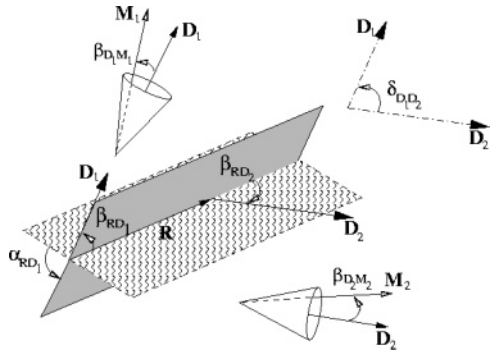

Figure 1. Coordinate systems and angles needed for describing electronic energy migration within a donor pair. The electronic transition dipole moments of the donors (D_1 and D_2) are coinciding with the *z*-axis of the molecular frames $\mathbf{M_1}$ and $\mathbf{M_2}$. The donors are assumed to be uniaxially oriented about the *z*-axis of the director frames $\mathbf{D_1}$ and $\mathbf{D_2}$, which are attached to a rigid macromolecule. The concept configuration here means the orientation of $\mathbf{D_1}$ and $\mathbf{D_2}$ with respect to the **R**-frame, which is defined by the three orienting angles (β_{RD_1}, α_{RD_1}, and β_{RD_2}) because α_{RD_2} is taken to be 0. The *z*-axis of the **R**-frame connects the center of mass of D_1 and D_2 at distance *R*.

transition dipole attached to a macromolecule, various coordinate systems are needed as is outlined below as well as in Figure 1. In the following $\langle c(t)\rangle$ may denote the time dependence of the fluorescence anisotropy $\{r_{ij}(t)$, vide infra, eq 8$\}$ or excitation probability $\{\chi(t)\}$.

1. Sample initial coordinate pairs from an equilibrium distribution in the local $\mathbf{D}_i$-frame ($i = 1, 2$) (the distribution is given by the potential used). The donors are statistically independent.

2. For each initial point do the following. (a) Generate Brownian dynamics trajectories of vectors ($\hat{\mu}_1^D$, $\hat{\mu}_2^D$) where (μ_{ix}^D, μ_{iy}^D, μ_{iz}^D) is diffusing on a unit sphere. (b) Compute the value of the functions $\{c(t)\}$, which involves the orientational transformation from the $\mathbf{D}_i$ to the **R** frame by using the Euler matrix $\{\tilde{A}\}$ of $\hat{\mu}_i^R = \tilde{A}(\Omega_{RD_i})\hat{\mu}_i^D$. Here Ω_{RD_i} ($=\alpha_{RD_i}$, β_{RD_i}) denote the Euler angles.

3. Compute ensemble averages $\langle c(t)\rangle = (1/N)\Sigma c(t)$, where *N* is the number of trajectory pairs. The generated solution typically contains 100000 pairs of trajectories.

To fit the simulated result to experimental data, the Levenberg−Marquardt algorithm was used. For each iteration in the fitting procedure, steps 1−3 were performed, as is illustrated elsewhere.[6]

Potentials are used in four ways. For these models, a unit vector in Cartesian coordinates moves on a unit sphere affected by a stochastic force. Dissimilarities of the different models originate in the orientational potential that hinders the reorienting motion. All potentials are cylindrically symmetrical with respect to $\mathbf{D}_i$. To test the importance of choosing different orienting potentials, the cone and various Maier−Saupe potentials were examined.

Cone Potential. The reorienting motion is free BD motion on a unit sphere until the trajectories move outside a hard cone wall ($z(t) < \cos(\theta_c)$) where they are reflected. The simulation method is presented elsewhere.[13]

Maier—Saupe Potential. The Maier−Saupe potential enables one to describe more complex reorientational dynamics, such as nonexponential rotational correlation functions, which may be observed for donor groups attached to protein molecules. Here different combinations of Maier−Saupe potentials are used. These are defined by Wigner rotation matrix elements, scaled to energy by ϕ. In this work, the first, second and fourth rank elements are used to define the total potential.

$$U_1(\beta) = \phi_1 P_1(\cos\beta) = \phi_1 \cos\beta$$

$$U_2(\beta) = \phi_2 P_2(\cos\beta) = \frac{\phi_2}{2}(3\cos^2\beta - 1)$$

$$U_3(\beta) = \phi_3 P_4(\cos\beta) = \frac{\phi_3}{8}(3 - 30\cos^2\beta + 35\cos^4\beta)$$

$$U(\beta) = U_1(\beta) + U_2(\beta) + U_3(\beta) \qquad (1)$$

The initial coordinates are generated using the rejection method.[14] Accepted coordinates fulfill the equilibrium probability density

$$p(\beta) = \exp(-U(\beta))/Z \qquad (2)$$

where *Z* denotes the partition function.

The numerical scheme uses a 3D diffusion process restricted to the two-dimensional surface of a sphere. Cartesian coordinates are used and the potential (cf. eq 1), written in transformed coordinates introduces a deterministic force $\nabla U(X)$ in the BD-simulation. The numerical scheme is explained further in Appendix A.

Combined Potentials. To describe complex reorienting motions of the D-groups, different linear combinations of potential functions were used. The key question was to create trajectories that accurately could describe reorientational functions. The intent was to find a flexible model that fulfilled this criterion, rather than providing a detailed physical explanation to the actual relaxation of the orientational correlation function. In the simulations performed, different terms of the Maier−Saupe potential of eq 1 were combined as follows:

1. All three terms U_1, U_2, U_3 were included.
2. Only the U_1 term was used.
3. Two diffusion processes were combined with two different U_1 potentials. In this approach, the potentials represented two independent motions of the molecular transition dipole relative to the director frame $\mathbf{D}_j$.

Deconvolution of Fluorescence Depolarization. In a true fluorescence experiment, the fluorescence decays depend on the width of the excitation profile, *E*(*t*). It is therefore necessary, in a simulation method, to convolute the simulated fluorescence decays with the excitation profile. The method was outlined in detail by Edman et al.[6] and briefly works as follows: The fluorescence intensities $F_{VV}(t)$ and $F_{VH}(t)$ can be calculated from the simulated $r(t)$ according to

$$F_{VV}(t) = f(t)[1 + 2r(t)]$$

$$F_{HV}(t) = f(t)[1 - r(t)] \qquad (3)$$

where $f(t)$ describes the fluorescence relaxation which is determined in a separate experiment. A difference curve $\{d(t) = F_{VV}(t) - F_{VH}(t)\}$ is then constructed and convoluted with the excitation profile

$$D(t) = \int_0^t E(t - t')\, \mathrm{d}(t')\, \mathrm{d}t' \qquad (4)$$

and compared with a experimental difference curve constructed from I_{VV} and I_{VH} ($D_{exp}(t) = I_{VV} - I_{VH}$). The goodness of fit is judged by performing a reduced χ^2 and weighted-residual analyses.[15]

Synthetic Data. To mimic time-correlated single photon counting (TCSPC) experiments, we have generated synthetic

data as described by Chowdhury et al.[16] Data sets were constructed so that the difference curve contained 50.000 counts in the peak maximum channel. The number of channels was 1024 and corresponded to a time-resolution of 50 ps per channel. The excitation pulse was taken to be a Gaussian function with full width at the half-maximum of 1.0 ns. When I_{VV} and I_{VH} are generated, the fluorescence relaxation was taken to be the sum of two exponential functions ($A_1 = 0.5$, $\tau_1 = 4.5$, $A_2 = 2.5$, $\tau_2 = 5.6$). These parameters were the same throughout all the experiments. In experiments using flash lamp pulses, or other pulse sources that produce nonsymmetric response functions, one can use the pulse shape previously proposed by Arcioni and Zannoni.[17] For the pulse width chosen in the present study, the selected pulse shape would not influence the results.

Theoretical Considerations

Fluorescence Anisotropy. From fluorescence depolarization experiments, it is possible to construct the fluorescence anisotropy,[18] which is an orientational correlation function of second rank. By using pulsed polarized excitation light on samples and then measuring the time-resolved polarized fluorescence relaxation, one can construct the time-resolved fluorescence anisotropy. The fluorescence anisotropy of an ensemble of fluorescent molecules is given by

$$r(t) = r_0\langle P_2[\hat{\mu}(0)\cdot\hat{\mu}(t)]\rangle \tag{5}$$

In eq 5 $\langle\cdots\rangle$ stands for the orientational average over the ensemble, and P_2 is the second Legendre polynomial. The orientation of the electronic transition dipole moment at the times of excitation and emission are denoted by the unit vectors $\hat{\mu}(0)$ and $\hat{\mu}(t)$, respectively.

Fluorescence Anisotropy and DDEM. Donor−donor energy migration (DDEM) between chemically and photophysically identical fluorophores can only be monitored by fluorescence depolarization experiments. In the following we consider two interacting donor groups (D_1 and D_2), which are both attached to a macromolecule. The macromolecule is assumed to undergo negligible reorientation on the fluorescence time scale. Because of energy migration between D_1 and D_2, the experimental fluorescence anisotropy $\{r(t)\}$ is composed of the following contributions;

$$r(t) = \frac{r(0)}{2}[\rho_1(t) + \rho_2(t) + \rho_{12}(t) + \rho_{21}(t)] \tag{6}$$

The fluorescence anisotropy of each donor in the absence of DDEM is given by $r_j(t)$ ($j = 1$ or 2). The anisotropy contribution caused by DDEM from D_i to D_j is denoted $\rho_{ij}(t)$.

The probability of being the initial excited donor is equal for D_1 and D_2 and the corresponding time dependence is $\chi(t)$. The anisotropy constitutes the following contributions:

$$\rho_i(t) = \langle P_2[\hat{\mu}_i(0)\cdot\hat{\mu}_i(t)]\chi(t)\rangle, \quad i = 1, 2 \tag{7}$$

$$\rho_{ij}(t) = \langle P_2[\hat{\mu}_i{}^R(0)\cdot\hat{\mu}_j{}^R(t)](1-\chi(t))\rangle, \quad i = 1, 2\ (i \neq j) \tag{8}$$

In eq 8, the superfix indicates an orientational transformation with respect to a coordinate system, which is fixed in the macromolecule (see Figure 1 and computational methods, step 2). The equation describing the excitation probability of the initially excited donor group is expressed as a function of the rate of energy migration (ω) given by[5]

$$\chi(t) = \frac{1}{2}[1 + \exp(-2\langle\omega\rangle t - 2\int_0^t[\omega(t') - \langle\omega\rangle]\,dt')]$$

$$\chi(0) = 1$$

$$\langle\omega\rangle = \lim_{T\to\infty}\frac{1}{T}\int_0^T\omega(t')\,dt' \tag{9a}$$

$$\omega(t') = \Lambda\kappa^2(t')$$

$$\Lambda = \frac{3}{2\tau}\left(\frac{R_0}{R}\right)^6$$

$$\kappa(t') = \hat{\mu}_1{}^R(t')\cdot\hat{\mu}_2{}^R(t') - 3(\hat{\mu}_1{}^R(t')\cdot\hat{R})\,(\hat{\mu}_2{}^R(t')\cdot\hat{R}) \tag{9b}$$

The strength of coupling, the Förster radius, and the fluorescence lifetime are denoted by Λ, R_0, and τ, respectively. In the following, the concept "extended Förster theory (EFT)" of donor−donor energy migration is defined by eqs 6−9.

Equation 9a is the formal solution to the stochastic master equation (SME), which was previously derived from the stochastic Liouville equation.[5] These equations account for the molecular origin to the stochastic transition rates. Recently numerical tests have shown that the SME provides an accurate description of the energy migration process under most experimental conditions of interest.[19] In practice the stochastic dependence of eqs 6−9 complicates the analyses of experimental data. This can be overcome by generating adequate stochastic orientational trajectories and by forming averages over a large number them (typically ~ 100000; see Computational Methods). Suitable potentials are required for generating trajectories. Some basic principles for this procedure have been described elsewhere.[6,7]

Cumulant Series Expansion of EFT. The stochastic time dependence of eqs 6−9 may be circumvented, provided suitable approximations are available, which in turn make analytical expressions obtainable. If one assumes that reorientational processes are statistically separated from the excitation probabilities, eqs 7 and 8 can be written as

$$\rho_i{}^{sep}(t) = \langle P_2[\hat{\mu}_i(0)\cdot\hat{\mu}_i(t)]\rangle\langle\chi(t)\rangle, \quad i = 1, 2 \tag{10}$$

$$\rho_{ij}{}^{sep}(t) = \langle P_2[\hat{\mu}_i{}^R(0)\cdot\hat{\mu}_j{}^R(t)]\rangle\langle(1-\chi(t))\rangle, \quad i = 1, 2\ (i \neq j) \tag{11}$$

The excitation probability is simplified considerably by adopting a cumulant series expansion, truncated at the first $\{\chi_1{}^{(1)}(t)\}$ and second $\{\chi_1{}^{(2)}(t)\}$ orders.[5] These procedures yield

$$\langle\chi_1{}^{(1)}(t)\rangle = \xi(t)\{1 + \exp(-2\langle\omega\rangle t)\}$$

$$\langle\chi_1{}^{(2)}(t)\rangle = \xi(t)\{1 + \exp(-2\langle\omega\rangle t)\exp(-2\int_0^t(t-t')\{\langle\omega(t')\omega(0)\rangle - \langle\omega\rangle^2\})\,dt'\}$$

$$\xi(t) = {}^1/_2\exp(-t/\tau) \tag{12}$$

To evaluate eq 12, the average $\langle\omega\rangle$ and the correlation function $\langle\omega(t')\omega(0)\rangle$ must be worked out. Details of this procedure are given elsewhere.[5]

Coordinate Frames. As previously mentioned, the D-groups considered are covalently bonded to a macromolecule, such as a protein. Each D-group is assumed to undergo reorientational motions, which are locally restricted, so that the orientational distribution of the electronic transition dipole is effectively uniaxial. To describe the orientation of each of the transition dipoles with respect to the macromolecule, two types of

coordinate systems (cf. Figure 1) are introduced. These are the director frames ($\mathbf{D}_j$) fixed to the macromolecule, and the fluorophore-fixed frames ($\mathbf{M}_j$), which describe the orientation of the transition dipole moment with respect to the $\mathbf{D}_j$-frame. A third frame (**R**), fixed in the macromolecule, is introduced so that its *Z*-axis interconnects the center of mass of each D-group (cf. Figure 1). Eulerian angles (Ω_{RD_j}) are used for orientational transformations between the $\mathbf{D}_j$- to **R**-frames.

Results and Discussion

The Cumulant Expansion: An Approximation of the EFT? Considerable simplification of the data analyses could be achieved provided that the analytical approximations of the EFT were valid. Previously, a series cumulant expansion was suggested.[5] This means that eq 12 gives the excitation probability for a first cumulant approximation of the EFT. However, fitting this approximate expression to experimental data only gives a value of $\langle\omega\rangle$, while the calculation of distances also requires a value of $\langle\kappa^2\rangle$. It is obvious that several configurations may correspond to the same $\langle\omega\rangle$ value. To illustrate the sensitivity of the configuration, we have studied three EFT-computations of the excitation probability. All of them correspond to the same $\langle\omega(t)\rangle$ value but represent different configurations. The deviation between approximate and EFT theory can be up to 25%, which strongly suggests that, in order to discriminate between different configurations, it is necessary to simulate and use the extended Förster theory. The deviation here means comparing the ensemble averages $\langle\chi(t)\rangle$ and $\langle\chi^{(1)}(t)\rangle$, which are given by eqs 9a and 12, respectively. The remaining part of this study will deal with the EFT.

The results presented below concern two aspects of the extended Förster theory when applied to fluorescence depolarization studies of energy migration within a pair of donors. One aspect is to explore whether distances between interacting donors can be accurately obtained, when using a more rigorous theory in the analyses of data. This question includes and should solve the so-called "κ^2-problem", which for years has been discussed by several scientists.[8] The second aspect deals with the stochastic dependence of the EFT, which demands a BD simulation. The BD simulation requires a potential function that effectively describes the orientational distribution of the donor group. For this purpose, the cone potential is a simple model, which is used in EPR spectroscopy for generating time-dependent orientational trajectories.[20] The Maier−Saupe potential is another choice, which is more attractive from a physical point of view. The choice of potential addresses the second aim of this work, namely to explore whether the choice of potential is crucial for the reliability of the extracted parameters.

The Parameter Space. Fluorescence depolarization experiments performed with interacting DD-pairs can often be restricted to eight parameters, if one assumes uniaxial orienting potentials (cf Figure 1) as well as parallel absorption and emission transitions dipoles. The latter is usually the case for $S_0 \leftrightarrow S_1$ transitions. Quite often one finds that the reorientational dynamics of a D-group in a protein, although complex, can be fitted to a monoexponential function. Within these assumptions the eight parameters are as follows: two potential parameters (the cone angle, or ϕ), two diffusion constants (cf. Appendix A), the strength of coupling (Λ) and the orientational configuration (β_{RD_1}, α_{RD_1}, β_{RD_2}). The order parameters and the rotational correlation times can be obtained from two independent experiments, one for each D-labeled biomacromolecule. Independent information about the configuration can be obtained from the limiting anisotropy of the DD-labeled

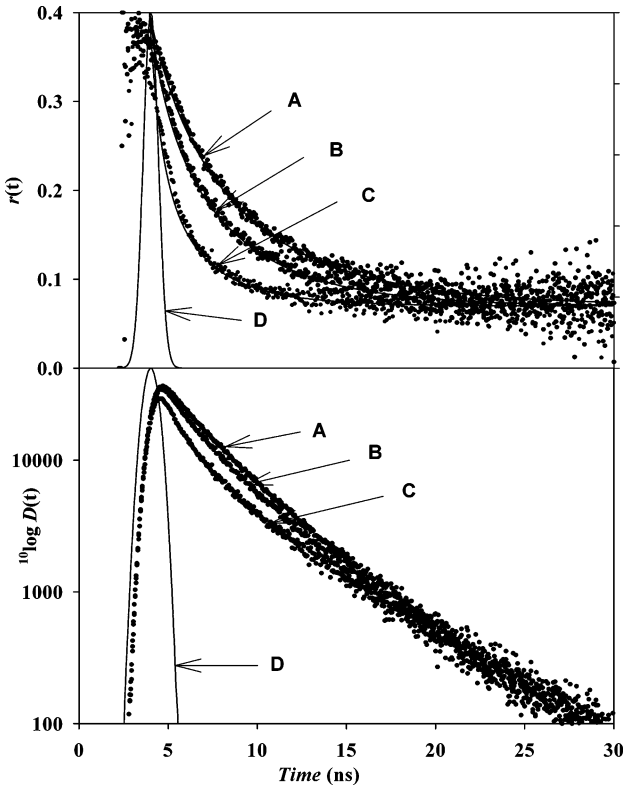

Figure 2. Fluorescence depolarization decays mimicking experimental data that were generated for three different configurations: (A) $\{\alpha_{RD_1} = 81.9°\}$, (B) $\{\beta_{RD_1} = 33.0°, \beta_{RD_2} = 73.5°, \alpha_{RD_1} = 99.2°\}$; (C) $\{\beta_{RD_1} = 21.0°, \beta_{RD_2} = 61.5°, \alpha_{RD_1} = 156.5°\}$. The cone angle, the rotational diffusion constant, the strength of coupling, and the angle between the *z*-axes of the $\mathbf{D_1}$ and $\mathbf{D_2}$ frames were the cone angle $\theta_c = 30°$, $D_k = 0.02$, $\Lambda = 0.5$ and $\delta_{D_1D_2} = 81°$, respectively. The lower curves show the fluorescence difference curves. In real experiments, usually the difference curve is created, deconvoluted, and analyzed to obtain the fluorescence anisotropy decays. The latter are displayed in the upper panel. The excitation profile is also indicated by the graphs in part D.

system (cf. eq 8), which is given by

$$\rho_{12}(t \rightarrow \infty) = \frac{1}{2} D_{00}^{2}(\delta_{D_1D_2}) \langle D_{00}^{2}(\beta_{D_1M_1}) \rangle \langle D_{00}^{2}(\beta_{D_2M_2}) \rangle \quad (13)$$

Here $\delta_{D_1D_2}$ denotes the angle between the *z*-axes of the $\mathbf{D}_j$-frames. The azimutal angle α_{RD_1} is related to β_{RD_1}, β_{RD_2}, and $\delta_{D_1D_2}$ according to

$$\alpha_{RD_1} = \arccos\{(\cos\delta_{D_1D_2} - \cos\beta_{RD_1}\cos\beta_{RD_2}) \times (\sin\beta_{RD_1}\sin\beta_{RD_2})^{-1}\} \quad (14)$$

Thus, the parameters describing the strength of coupling (Λ) and the configuration $\{\delta(\beta_{RD_1}, \alpha_{RD_1}, \beta_{RD_2})\}$ remain to be obtained from the analyses of the time-resolved depolarization data. Actually the *functional shape* of the fluorescence depolarization decays contains this information. To illustrate this fact, depolarization data were generated representing the same coupling strength, but with different configurations. The results are displayed in Figure 2. The shape of the fluorescence difference curves as well as the anisotropy decays is clearly dependent on the configuration. The coupling strength $\Lambda = 0.5$ means that the interacting donor groups are separated by about one Förster radius. The reason the shapes of the depolarization data are sensitive to the configuration is explained by the orientational correlation between the interacting molecules. This is manifested in the third and fourth terms of eq 6, but is even

more evident from eq 8. The influence of configuration on the correlation is further analyzed elsewhere.[21] Although information about the configuration is present in the depolarization data, this information is not necessarily easily extracted by the data analyses. However, the determination of the configuration can be improved considerably by simultaneously analyzing data obtained under different conditions, where the configuration and coupling strength are invariant. However, the order parameters as well as the reorientational rates are varied. For instance, such data might correspond to different temperatures or dissolving the biomacromolecule in various solvent mixtures.

General Procedure for Analyzing Depolarization Data. Any optimal analysis of a DD-system requires independent data from the two corresponding D-systems. Taken together, these three experiments represent a set of data. Before starting the EFT-analyses of the DD-system, the time-resolved fluorescence anisotropy data obtained for the two D-systems are used to create the properties of the orientational potential. For each D-system the properties of a selected orienting potential are adjusted as to fit the dynamic (i.e. the rotational correlation times) and static (i.e. the second rank order parameters) properties of the anisotropy decay. To achieve this goal, different orientational trajectories are generated and examined until the best fit to experiments is obtained. In the present work, synthetic data were generated corresponding to large variety of configurations and coupling strengths. The detailed procedure for creating trajectories is given above in the section Computational Methods. Once having obtained the orientational trajectories for each D-group, the analysis of the DD-experiment can start. This means searching for the best fit of the EFT with respect to the coupling strength and the configuration parameters. Further details concerning the simulation−deconvolution procedure are given elsewhere.[6] It is recommended to use two or more data sets to obtain a more stable analysis of the data, as is briefly mentioned in the previous subsection. For instance, the data may be recorded at different temperatures or for different solvent composition. All data sets are then analyzed in a global manner, because several parameters are assumed to be common for the different data sets.

Recovering Distances and Configurations. The EFT provides the accurate description of energy migration within a DD-pair. To judge the reliability of analyzing data with the EFT, an immense number of experimental data was generated representing different configurations as well as different coupling strengths. The regime of coupling and the results in error of distance and configuration are presented as a function of a dimensionless parameter

$$\vartheta = \tau_c\sqrt{\langle\omega^2\rangle - \langle\omega\rangle^2} \qquad (15)$$

that measures the dynamical influence on the coupling strength. Values of $\vartheta \approx 0.1$, $\vartheta \approx 1$, and $\vartheta \approx 10$ represent weak, intermediate, and strong coupling, respectively, that cause slow, intermediate, and fast components of the fluorescence depolarization decay. The ϑ value is also referred to as the Kubo number.[22] In practice, a study covering all possible configurations is not possible. For this reason we have focused on investigating parts of the configuration space that represent extreme values, a variety of order parameters, rates of donor reorientation, and coupling strengths. The results obtained for different ϑ values are displayed in Figure 3. The errors in distance and configuration as a function of ϑ are summarized in Figure 3A and 3B, respectively. For a wide range of cases the errors in distance are typically less than 5% over the range

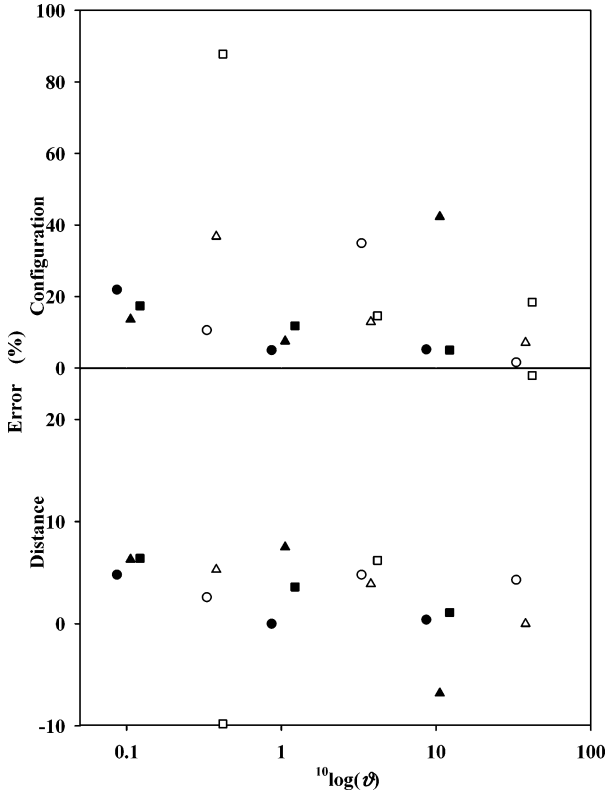

Figure 3. Errors (%) in the distance and configuration parameters obtained from the simulation−deconvolution analyses. The errors in configuration, i.e. (β_{RD_1}, α_{RD_2}, and β_{RD_2}) and distance are presented in the upper and lower panels, respectively. Two different sets of data were generated, corresponding to low (filled symbols) and high (empty symbols) stochastic noise. The data indicated by □, △, and ○ correspond to the angle $\delta = 9°$, 54.7° and 80°, respectively. The error of configuration was calculated according to $^1/_3\{(|[\beta_{RD_1}{}^{calc} - \beta_{RD_1}{}^{true}]/\beta_{RD_1}{}^{true}|) + (|[\beta_{RD_2}{}^{calc} - \beta_{RD_2}{}^{true}]/\beta_{RD_2}{}^{true}|) + (|[\alpha_{RD_2}{}^{calc} - \alpha_{RD_2}{}^{true}]/\alpha_{RD_2}{}^{true}|\}$.

$0.1 < \vartheta < 10$, while the errors in configuration are larger. The results shown were obtained for two sets of experiments corresponding to, e.g., two different temperatures. Data were analyzed in a global manner. Although the configuration accuracy is not as good, the small errors in distance are encouraging, since the distance information is of primary interest in most applications. The ϑ value depends on the configuration. To illustrate this, the ϑ-number is displayed in Figure 4 as a function of the configurations, which are limited by two fixed values on the $\delta_{D_1D_2}$-angle. This angle was chosen to be 80 and 9°. Moreover, one should notice that the configuration obtained is not unique due to symmetry.

Different Orienting Potentials. In mimicking fluorescence depolarization data obtained by the TCSPC technique, two potential models were used, namely the cone and the Maier−Saupe potentials. The cone potential, which is often used to model anisotropic motions, appears somewhat artificial as compared to the more physically tractable Maier−Saupe potential. To test whether the EFT analyses are sensitive to the choice of potential, orientational trajectories were generated by means of the Maier−Saupe potential. The generated TCSPC data were then re-analyzed by using the Maier−Saupe as well as the cone potentials. The generated depolarization experiments correspond to Kubo numbers ranging over $0.1 < \vartheta < 10$, which means weak, intermediate, and strong coupling.

Typical results of such a study for data generated with the U_1 potential (cf. the subsection Combined Potential, case 2) are presented in Figure 5. Similar errors in distance were obtained

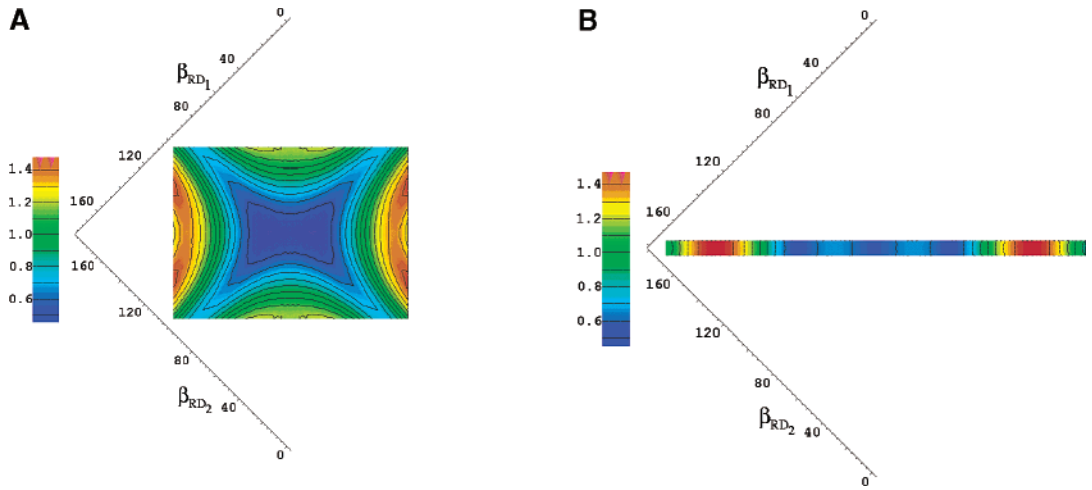

Figure 4. Dynamical influence on coupling strength (ϑ) as a function of configuration: (A) $\delta_{D_1D_2} = 80°$; (B) $\delta_{D_1D_2} = 9°$. Possible configurations for a given $\delta_{D_1D_2}$ are bounded by $|\beta_{RD_1} - \beta_{RD_2}| \leq \delta_{D_1D_2}$ and $(\beta_{RD_1} - \beta_{RD_2}) \geq \delta_{D_1D_2}$. For cases A and B, order parameters are $S = 0.81$.

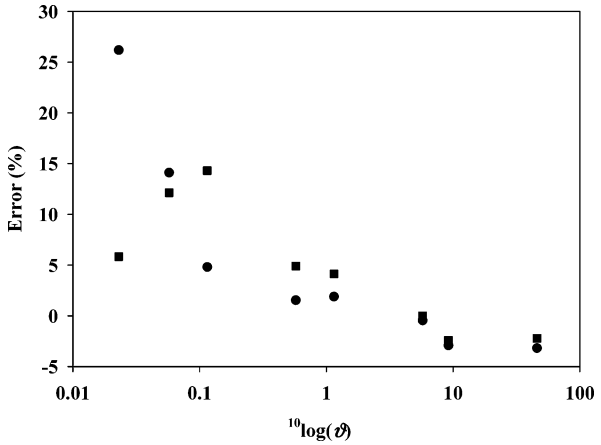

Figure 5. Error in distance (%) obtained from simulation−deconvolutions using the Maier−Saupe $U_1(\beta)$-potential (■) and a cone potential (●). The data were generated with Maier−Saupe potential using the configuration $\alpha_{RD_1} = 76.7°$ and $\beta_{RD_1} = \beta_{RD_2} = 60.0°$ for couplings strengths of $0.005 < \Lambda < 10.0$. For the reorientational part, $\phi_1 = 6$ and $D_k = 0.03$ which corresponds to a cone angle of 33.4°. Greatest difference between cone and Maier−Saupe potential is obtained for low cone angles.

when generating and re-analyzing data with a Maier−Saupe potential that includes three potential terms (cf. the subsection Combined Potential, case 1), and by using two diffusion processes combined with two different U_1 potentials (cf. the subsection Combined Potential, case 3).

Conclusions

The present and previous works show that approximate and analytical expressions of EFT obey a very limited validity. Unlike approximate models, the EFT accounts for the correlation between reorienting motions and electronic coupling between the interacting donors. Interestingly, not only the strength of coupling, which enables distance calculations but also the orientational configuration of the interacting donors could be extracted from the shape of the depolarization decay. In all approximate models used, the orientational configuration usually introduces uncertainties in the calculation of distances. Even if the accuracy of determining the unique configuration by EFT is less than good, the κ^2-dynamics is considered in detail, which is not the case in any other existing model. Furthermore, combining data recorded under different conditions (e.g., different temperatures and solvent viscosities) in a global manner should increase the accuracy in determining the distance as well as the configuration. The idea would then be that the local dynamics change, while the configuration remains the same. Hence several sets of independent data are obtained, which contain the same information about the migration process and thus increase the statistical accuracy. One problem with this approach could be that the global motions of the protein molecule start to contribute upon increasing temperature (or decreasing viscosity). Hereby a solution is given to the long lasting problem of handling the κ^2 dependence of the migration/transfer rate. This problem also remains to be solved for DAET and PDDEM, which is a work in progress.

Taken together, combining EFT and various MD simulations must be performed to achieve the most accurate analyses of DDEM experiments. Using the EFT as presented here brings the analyses of DDEM data to the same level of molecular detail as in ESR- and NMR-spectroscopy. This means that the *macroscopic* information, i.e., the experimental data, is related to the *microscopic* picture, i.e., the electronic dipole−dipole coupling and that the analyses then yield molecular parameters like rotational correlations times, order parameters, and intermolecular distances.

Acknowledgment. We are grateful to the Swedish Research Council and the Kempe Foundations for financial support.

Appendix A

Simulations Using a Mean-Field Potential. A numerical scheme for BD simulation in a mean field potential is presented. The problem is solved with an Ito diffusion equation.[23] The presented method is tested in a convergence analysis and is also put into context of other BD-simulation methods.

The Ito formalism gives a convenient framework to derive numerical schemes at any order of accuracy, several of them are listed elsewhere.[24] The schemes can be conveniently expressed in FORTRAN or C-code using MAPLE.[25] In this work, we are interested in the reorientational motion of fluorescent molecules influenced by a surrounding that leads to restricted motional freedom. Formulating an Ito equation for diffusion on a sphere, where a mean field potential causes the deterministic force, solves this problem.

The problem of reorientation is solved using a 3D diffusion process, which is restricted to a 2D surface ($F(X) = 0$). A stochastic differential equation of the form $dX = A(X)\,dt + B(X)\,dW$ is formulated by Persson et al.[23] where the conditions

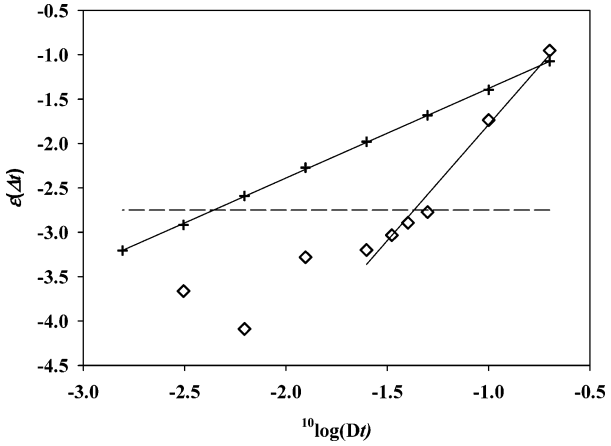

Figure 6. For potential $U_1(\beta)$ with $\phi_1 = 5$, the logarithmic error of the second rank order parameter $\epsilon(\Delta) = {}^{10}\log(|S - S(X^{\Delta})|)$. S is calculated analytically and $S(X^{\Delta})$ is sampled using BD-simulations ($\sim$ 500000-trajectories) with different time steps. Results obtained when using the first-order weak Euler scheme is indicated with a + and the wktay2 scheme with a ◇. The dashed line represents the estimated statistical error for this number of trajectories.

that the drifts vector $A(X)$ and diffusion matrix $B(X)$ must fulfill in order for this to be an Ito diffusion process on $F(X) = 0$ are stated. This formulation is tested in numerical schemes in[26] for the case of free diffusion (i.e. no deterministic force included) on different 2D surfaces $F(X) = 0$. The matrix $B(X)$ guarantees that the stochastic process is in the tangent planes of F. For the case of free diffusion on $F(X) = 0$ the drifts vector has the following form:

$$A = -\frac{1}{2} tr(B \nabla \nabla^T F) \frac{\nabla F}{||\nabla F||^2} \qquad \text{(A1)}$$

It also serves the task of keeping the diffusion processes on $F(X) = 0$. The numerical scheme used[26] is here generalized to include a potential $U(X)$. The drifts vector is generalized by using

$$A(X) \rightarrow A(X) + \nabla U(X) \qquad \text{(A2)}$$

Note that the condition $\nabla U(X) \cdot \nabla F(X) = 0$ is sufficient for $X(t)$ to be an Ito process on $F(X) = 0$.[23,26] This implies that any type of potential of pure angular dependence such as the Maier−Saupe potential can be used because $\nabla U(X) \perp \nabla F(X)$. The convergence of a BD-simulation method including a deterministic force ($\nabla U(X)$) is tested for diffusion on a sphere with

$$F(X) = \frac{1}{2}((X^{(1)})^2 + (X^{(2)})^2 + (X^{(3)})2 - 1) = 0 \qquad \text{(A3)}$$

when using a weak Euler numerical scheme, as well as a weak explicit second-order Taylor scheme, denoted wktay2 (see ref 24, p 466). The weak Euler scheme has the form

$$X_{n+1} = X_n + A(X_n)\Delta t + B(X_n)\Delta W_n \qquad \text{(A4)}$$

where $X = (X^{(1)}, X^{(2)}, X^{(3)})$ and ΔW_n stands for a 3D-random number vector that can be Gaussian, or two point random numbers $P(\Delta W_n^{\alpha} = \sqrt{\Delta t}) = {}^1/_2$.[24] Here $\Delta t = D_k h$, where the diffusion coefficient is D_k and h denotes the time/channel.

For the data shown in Figure 6 the potential $U_1(X)$ from eq 1 (with $\phi = 5$) was used. The errors obtained in the simulation of second rank order parameters ($\langle D_{00}^{(2)}(\beta_{D_j M_j})\rangle$, $j = 1,2$) are given for different time steps (Δt). Notice that in using the Euler scheme (+) one reaches convergence of first order, as is expected,[24] while the wktay2 scheme exhibits slightly stronger convergence properties than second order. One cannot, of course, obtain better results than the estimated statistical errors (dashed line in Figure 6 for 500000 trajectories). The error of 10^{-3} in the order parameters using the Euler and the wktay2 scheme is obtained in simulations lasting 4 min 40 s and in 2 min 50 s, respectively. This means that second-order scheme is more efficient because a small error can be obtained using a longer time step. Despite this fact, the Euler scheme is preferred because in order to represent a typical experiment spanning 1024 data points and demanding an error of 10^{-3}, it is in practice less time-consuming as compared to wktay2.

Abbreviations

A = acceptor of electronic energy
BD = Brownian dynamics
D = donor of electronic energy
D_j = the jth donor
D_j = the rotational diffusion constant of the jth donor
$D(t)$ = difference curve created from fluorescence depolarization experiments
$\mathbf{D_j}$ = director frame for the jth donor
DAET = donor−acceptor energy transfer
DDEM = donor−donor energy migration
EFT = extended Förster theory
EM = energy migration
FRET = fluorescence resonance energy transfer
L = laboratory frame
$\mathbf{M_j}$ = molecule fixed frame for the j-th donor
MD = molecular dynamics
PDDEM = partial donor−donor energy migration
R = the distance between the donor groups
R = coordinate system fixed in a protein
S_j = second rank order parameter of the jth donor
TCSPC = time-correlated single-photon counting
τ = the fluorescence lifetime

References and Notes

(1) Wilczynska, M.; Fa, M.; Karolin, J.; Ohlsson, P.-I.; Johansson, L. B.-Å.; Ny, T. *Nature: Struct. Biol.* **1997**, *4*, 354.
(2) Hägglöf, P.; Bergström, F.; Wilczynska, M.; Johansson, L. B.-Å.; Ny, T. *J. Mol. Biol.* **2004**, *335*, 823.
(3) Johansson, L. B.-Å.; Bergström, F.; Edman, P.; Grechishnikova, I. V.; Molotkovsky, J. G. *J. Chem. Soc., Faraday Trans.* **1996**, *92*, 1563.
(4) Karolin, J.; Fa, M.; Wilczynska, M.; Ny, T.; Johansson, L. B.-Å. *Biophys. J.* **1998**, *74*, 11.
(5) Johansson, L. B.-Å.; Edman, P.; Westlund, P.-O. *J. Chem. Phys.* **1996**, *105*, 10896.
(6) Edman, P.; Håkansson, P.; Westlund, P.-O.; Johansson, L. B.-Å. *Mol. Phys.* **2000**, *98*, 1529.
(7) Edman, P.; Westlund, P.-O.; Johansson, L. B.-Å. *Phys. Chem. Chem. Phys.* **2000**, *2*, 1789.
(8) Van der Meer, B. W.; Coker, G.; III; Chen, S.-Y. S. *Resonance Energy Transfer: Theory and Data*; VCH Publishers: Weinheim, Germany, 1994.
(9) Dale, R. E.; Eisinger, J. *Biopolymers* **1974**, *13*, 1573.
(10) Maier, W.; Saupe, A. *Z. Naturforsch. A* **1959**, *14*, 882.
(11) Doi, M. *J. Polym. Sci. Polym. Phys. Ed.* **1981**, *19*, 229.
(12) Öttinger, H. C. *Stochastic processes in polymeric fluids*; Springer: Berlin, Heidelberg, Germany, and New York, 1996.
(13) Fedchenia, I.; Westlund, P.-O.; Cegrell, U. *Mol. Simul.* **1993**, *11*, 373.
(14) Press, W. H.; Teukolsky, S. A.; Flannery, B. P. Cambridge University Press: Cambridge, England, 1992.
(15) Demas, J. N. *Excited-state lifetime measurements*; Academic Press: New York, 1983.
(16) Chowdhury, F. N.; Kolber, Z. S.; Barkley, M. D. *Rev. Sci. Instrum.* **1991**, *62*, 47.
(17) Arcioni, A.; Zannoni, C. *Chem. Phys.* **1984**, *88*, 113.
(18) Lakowicz, J. R. *Principles of Fluorescence Spectroscopy*, 2nd ed.; Kluwer Academic/Plenum Publishers: New York, 1999.

(19) Håkansson, P.; Westlund, P.-O. *Spectrochim. Acta A* **2004**, in press.
(20) Liang, Z.; Westlund, P.-O. *J. Chem. Phys.* **1993**, *99*, 7090.
(21) Håkansson, P. *Simulation of Relaxation Processes in Fluorescence, EPR and NMR Spectroscopy*.
(22) Kampen, N. G. v. *Stochastic Prcesses in Physics and Chemistry*; Amsterdam, 1981.
(23) Persson, L.; Cegrell, U.; Usova, N.; Westlund, P.-O. *J. Math. Chem.* **2002**, *31*, 65.
(24) Kloeden, P. E.; Platen, E. *Numerical Solution of stochastic Differential Equations*; Springer-Verlag: Berlin, 1992.
(25) Cyganowski, S.; Kloeden, P.; Ombach, J. *From Elementary Probability to Stochastic Differential Equations with MAPLE*; Springer-Verlag: Berlin, 2002.
(26) Håkansson, P.; Persson, L.; Westlund. P.-O. *J. Chem. Phys.* **2002**, *117*, 8634.